

StyleSeg V2: Towards Robust One-shot Segmentation of Brain Tissue via Optimization-free Registration Error Perception

Zhiwei Wang¹, Xiaoyu Zeng¹, Chongwei Wu¹, Jinxin Lv¹, Xu Zhang², Wei Fang² and Qiang Li¹

¹HuaZhong University of Science and Technology

²Wuhan United Imaging Healthcare Surgical Technology

{zwwang, zengxiaoyu, chongweiwu}@hust.edu.cn, lvjinxin@vivo.com, xu.zhang@uih-surgical.com, muzili225@126.com and liqiang8@hust.edu.cn

Abstract

One-shot segmentation of brain tissue requires training registration-segmentation (reg-seg) dual-model iteratively, where reg-model aims to provide pseudo masks of unlabeled images for seg-model by warping a carefully-labeled atlas. However, the imperfect reg-model induces image-mask misalignment, poisoning the seg-model subsequently. Recent StyleSeg bypasses this bottleneck by replacing the unlabeled images with their warped copies of atlas, but needs to borrow the diverse image patterns via style transformation. Here, we present StyleSeg V2, inherited from StyleSeg but granted the ability of perceiving the registration errors. The motivation is that *good registration behaves in a mirrored fashion for mirrored images*. Therefore, almost at no cost, StyleSeg V2 can have reg-model itself “speak out” incorrectly-aligned regions by simply mirroring (symmetrically flipping the brain) its input, and the registration errors are symmetric inconsistencies between the outputs of original and mirrored inputs. Consequently, StyleSeg V2 allows the seg-model to make use of correctly-aligned regions of unlabeled images and also enhances the fidelity of style-transformed warped atlas image by weighting the local transformation strength according to registration errors. The experimental results on three public datasets demonstrate that our proposed StyleSeg V2 outperforms other state-of-the-arts by considerable margins, and exceeds StyleSeg by increasing the average Dice by at least 2.4%.

1 Introduction

Brain tissue segmentation is a fundamental technique in clinical practice, which enables accurate disease diagnosis and treatment planning [Geuze *et al.*, 2005]. The existing fully supervised segmentation methods can achieve promising segmentation accuracy with sufficient well-annotated data. However, the sophisticated brain structure makes the 3D manual annotation of brain MRI images labor-intensive and error-prone. Therefore, training a segmentation method using only a few labeled images is of great practical significance.

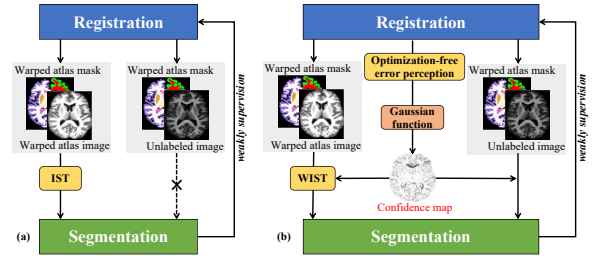


Fig. 1: The schematic diagram of (a) StyleSeg and (b) StyleSeg V2.

A straightforward solution is called atlas-based segmentation [Lorenzo-Valdés *et al.*, 2002; Lötjönen *et al.*, 2010]. The key idea is to first establish a pixel-wise correspondence between a carefully-labeled atlas image (moving image) and an unlabeled image (fixed image) through unsupervised registration based on image-level similarity, and then the mask of atlas can be propagated as the segmentation result.

However, the registration model pays more attention to an overall spatial accordance instead of the specific brain tissue of interest, which therefore leads to sub-optimal segmentation results [He *et al.*, 2020]. In comparison, a more effective paradigm proposed recently is to jointly learn two models for weakly supervised registration and semi-supervised segmentation, which forms a dual-model iterative learning [He *et al.*, 2020; Beljaards *et al.*, 2020; Zhao *et al.*, 2019a; He *et al.*, 2022]. Concretely, a registration model (reg-model) is first trained purely relying on target-agnostic image-level similarity, providing pseudo masks of unlabeled images for supervising a segmentation model (seg-model); the learned seg-model then predicts refined masks to weakly supervise the reg-model, forcing it to pay more attention to the tissue of segmentation interest; in the next iteration the reg-model can warp better and thus enhance the seg-model predictably.

Despite their success, a common bottleneck occurs when using the reg-model to generate pseudo masks of unlabeled images. That is, the reg-model is certainly imperfect, thus yielding incorrectly-aligned regions in each image-mask pair. The seg-model could partly tolerate these misaligned regions thanks to the inductive ability, but eventually be unbearable as they iteratively accumulate.

To address the above bottleneck, StyleSeg [Lv *et al.*, 2023] was proposed as shown in Fig. 1(a). It rejects the image-mask pairs containing registration error, and takes a bypass by us-

ing the warped copies of atlas-mask pairs, that is, replacing the unlabeled image with the warped atlas image. However, StyleSeg has a major issue: the seg-model always “sees” the copies of the same atlas, ignoring the valuable information carried by the unlabeled images. Although StyleSeg designs image-aligned style transformation (IST) to borrow the varied image patterns from the unlabeled images, the registration error could also degrade the fidelity of the style-transformed atlas copies. Therefore, bypassing the registration error is just a compromise and could cause other implicit troubles eventually. A few studies, e.g., DeepRS, have tried to predict the registration error by mostly resorting to complex extra models like GAN, which, however, intensifies training costs on top of learning dual-model on 3D paired images.

In this paper, we introduce StyleSeg V2 as the next generation of StyleSeg. This upgraded version not only enhances the reliability of style-transformed atlas images but also permits the unlabeled images to join the training process effectively, as illustrated in Fig. 1(b). Specifically, StyleSeg V2 “awakens” the inherent yet often overlooked capability of the registration model to perceive registration error without relying on any learnable parameters. Motivated by the observation that the two symmetrical brain hemispheres often exhibit asymmetric registration error, StyleSeg V2 generates mirrored images by swapping the left and right brain parts symmetrically, and identifies error on the original image by checking the symmetrical consistencies of predictions on the mirrored one. By use of registration error, StyleSeg V2 reinvents IST as weighted IST (WIST) by reducing the style transformation force on the atlas image for those misaligned local regions, and moreover selects the low-error regions from the unlabeled images to directly constrain seg-model.

To summarize, our contributions are listed as follows:

- We propose StyleSeg V2 for robust one-shot brain segmentation, which distinguishes itself from the original StyleSeg by a power of perceiving registration errors almost effortlessly.
- We propose two enabling techniques on top of the perceived registration errors, i.e., weighted image-aligned style transformation and confidence guided Dice loss. The former enables StyleSeg V2 to “see” more diverse and high-fidelity style-transformed atlas image in the bypass training, and the latter boosts StyleSeg V2 directly using the correctly-aligned regions of unlabeled images.
- The experimental results on three public datasets demonstrate the superiority of StyleSeg V2 in both brain segmentation and registration. Compared to the original version, StyleSeg V2 improves the segmentation performance by increasing the average Dice by 2.0%, 2.4%, and 1.7% on the three datasets, respectively.

2 Related Works

2.1 Dual-model based one-shot brain segmentation

One-shot brain segmentation aims at using only a single labeled image (atlas) to train a segmentation model for brain tissues. The dual-model iteration strategy is one of the most typical and effective solutions. For example, DeepAtlas [Xu

and Niethammer, 2019] treated the reg-model as a data augmentation scheme to provide image-mask pairs for segmentation, and then utilized the seg-model to conversely guide the reg-model learning. Despite their success, the main issue is that the reg-model inevitably causes misalignment between the unlabeled image and registration-provided pseudo mask, misleading the seg-model subsequently. To address this, StyleSeg [Lv *et al.*, 2023] was proposed to apply a style transformation on atlas to equip it with more diverse patterns and directly used the warped copies of atlas-mask pair to train the seg-model. StyleSeg considered the Fourier amplitude spectrum of image mainly containing statistical information of style, and linearly mixed up the amplitude components between unlabeled image and warped one to generate the style-transformed atlas image. However, the style transformation is still negatively affected by registration error more or less, which makes the generated warped image is always accompanied with visual artifacts when the registered image pairs are not well aligned, and thus harms the segmentation learning.

2.2 Registration error perception

Registration error perception aims to find where the misalignment occurs in the results of a registration model. Some methods [Sokooti *et al.*, 2019; Sokooti *et al.*, 2021; Bierbrier *et al.*, 2022] tried to train a supervised model using synthetic data with known registration errors. However, the scalability of such methods are limited as the deformation in medical scenes is complex and hard to simulate. In view of this, there were a few methods [Mok and Chung, 2022] proposed a cycle-form registration from the moving image to the fixed, and then back to the moving itself. They assumed that a voxel with good registration will come back to the original position precisely in the cycle registration. Such manner only estimates the total error of twice registration (moving-fixed and fixed-moving), while the error in each of the two paths is still unknown. To perceive the error of once registration, the method [Saygili *et al.*, 2015] constructed a voxel-level cost space between the registered image pairs and designed an objective function to calculate the confidence map via optimization. DeepRS [He *et al.*, 2020] considered the reg-model as generator, and trained a discriminator to produce a pixel-wise confidence map based on adversarial learning. Nevertheless, these methods introduce an additional optimization task, resulting in heavy computing overhead and making the dual-model learning process more cumbersome.

3 Methods

3.1 Overview of iterative learning in StyleSeg V2

Fig. 2 illustrates StyleSeg V2, which involves training a registration model (reg-model) and a segmentation model (seg-model) in an iterative manner. At the beginning (iteration 0), StyleSeg V2 trains the reg-model for initialization by purely minimizing the image-level similarity between the warped and target images following the regular training paradigm as in the previous StyleSeg [Lv *et al.*, 2023].

In each iteration, the reg-model is firstly fixed, and warps a carefully-labeled atlas multiple times targeting to different unlabeled images, to provide the seg-model a pseudo mask

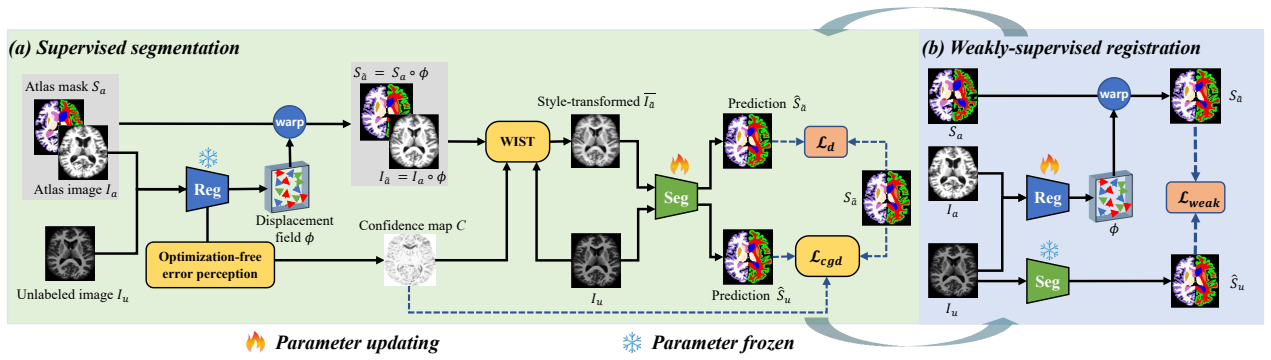


Fig. 2: The overview of iterative training in StyleSeg V2. (a) We first frozen reg-model to predict a pseudo mask (warped atlas mask) and a registration confidence map for supervising seg-model on both warped atlas image and unlabeled one. Weighted image-aligned style transformation style-transformed (WIST) increases both diversity and fidelity of the warped atlas image, and confidence guided Dice loss \mathcal{L}_{cgd} constrains the seg-model using the aligned regions of the unlabeled image. (b) We then fix the seg-model to produce a refined prediction of unlabeled image, which can be further exploited to weakly supervise the reg-model, triggering a new round of iteration

for each unlabeled one. A strategy of optimization-free error perception is designed to further calculate a confidence map, and each entry of the map indicates the probability of correctly-aligning for each position.

Then the seg-model can be trained by utilizing the pseudo mask to supervise the segmentation results of two images, i.e., the warped atlas image and the corresponding unlabeled image. For the warped atlas image, StyleSeg V2 uses the weighted image-aligned style transformation (WIST) based on the confidence map to increase the style diversity of the warped atlas image, and also to keep its image fidelity. For the unlabeled image which contains the real image patterns but imperfectly aligned with the pseudo mask, StyleSeg V2 also make use of it by introducing a confidence guided Dice loss to supervise the seg-model only using those correctly-aligned regions.

After the seg-model is trained, StyleSeg V2 fix it to predict finer pseudo masks of unlabeled images for retraining the reg-model using the regions of interest as auxiliary weak supervisions. Thus, the retrained reg-model can do a better warping in the next iteration.

In the following, we detail the three key steps in StyleSeg V2, i.e., optimization-free registration error perception, weighted image-aligned style transformation, and confidence guided Dice loss, and also give the implementation and training details.

3.2 Optimization-free registration error perception

Given the 3D atlas image I_a and an unlabeled one I_u , the reg-model predicts a displacement field ϕ and has $I_{\bar{a}} = I_a \circ \phi \rightarrow I_u$, where \circ is a simplified notation of warping, \rightarrow points to the warping target, and $I_{\bar{a}}$ is the warped image. We find that for symmetrical brain structures, the poor registration results exhibit strong non-symmetric characteristics at the left and right sides. Based on this phenomenon, StyleSeg V2 can force a learned reg-model to identify its own prediction errors without other extra optimization.

Specifically, StyleSeg V2 symmetrically flips the image along the sagittal axis in the 3D space to generate a fake image where the left and right brain parts are swapped. We de-

note such operation as “mirror” operation and distinguish the mirrored image using a superscript $*$. The atlas and unlabeled images are mirrored to get (I_a^*, I_u^*) and fed into the reg-model to predict a new displacement field ϕ' , yielding a warped mirrored atlas image $I_a^* \circ \phi' \rightarrow I_u^*$. We next mirror the resulting image back and combing the two times of warping as:

$$(I_a^* \circ \phi')^* \rightarrow (I_u^*)^* = I_u \leftarrow I_a \circ \phi \quad (1)$$

Therefore, we have $(I_a^* \circ \phi')^* \rightleftharpoons I_a \circ \phi$. A straightforward way of quantifying the registration errors is to calculate the voxel-level difference between $(I_a^* \circ \phi')^*$ and $I_a \circ \phi$. However, such manner could be too intensity sensitive to fully reveal the accurate spatial misalignment. To avoid this, StyleSeg V2 calculates the registration errors purely based on the displacement fields instead of voxel intensities.

The “mirror” operation can be mathematically expressed as a fixed displacement field ϕ_{mirr} defined as $\phi_{mirr}(x, y, z) = (N_x - 2x, 0, 0)$, where x is on the axis perpendicular to the symmetric plane, i.e., the sagittal plane, and N_x is the axis length. Therefore, Eq. (1) can be rewritten as $((I_a \circ \phi_{mirr}) \circ \phi') \circ \phi_{mirr} \rightleftharpoons I_a \circ \phi$. According to [Zhao *et al.*, 2019c], the multiple warping can be simplified as a single warping, and the relationship is that $((I_a \circ \phi_{mirr}) \circ \phi') \circ \phi_{mirr} = I_a \circ (\phi_{mirr} + (\phi' + \phi_{mirr} \circ \phi') \circ \phi_{mirr})$. Thus, we have the final equation:

$$I_a \circ \Phi \rightleftharpoons I_a \circ \phi \quad (2)$$

where $\Phi = \phi_{mirr} + (\phi' + \phi_{mirr} \circ \phi') \circ \phi_{mirr}$ is a displacement field equivalent to warping by use of ϕ_{mirr} , ϕ' and ϕ_{mirr} sequentially.

Using Eq. (2), the error map E of the original registration from the atlas to unlabeled image can be easily obtained by calculating the distance between the displacement vectors of Φ and ϕ , which is formulated as follows:

$$E = \|\Phi - \phi\|_2 \quad (3)$$

To normalize the registration error, we further convert E into a confidence map C ranged from 0 to 1 by using a Gaussian transfer function on the error map E , that is:

$$C = \exp\left(-\frac{E^2}{2\sigma^2}\right). \quad (4)$$

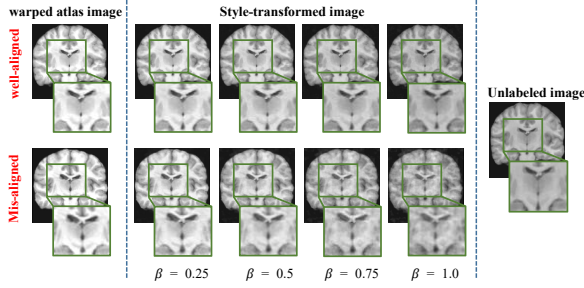


Fig. 3: The flaw of IST: artifacts appear if the images are mis-aligned due to imperfect registration, and become severer as the transformation strength goes higher.

where σ is the standard deviation of E . Each entry of C indicates a probability of the two images being well-aligned with each other at this position.

3.3 Weighted image-aligned style transformation for training with atlas

To avoid lacks of diversity, the original StyleSeg utilized image-aligned style transformation (IST) between $I_{\bar{a}}$ and I_u to produce style-diverse image $\bar{I}_{\bar{a}}$ for supervising the seg-model. The principle of IST is formulated as follows:

$$\bar{I}_{\bar{a}} = \mathcal{F}^{-1} \left((\beta \times \mathcal{A}(I_u) + (1 - \beta) \times \mathcal{A}(I_{\bar{a}})) e^{-j \times \mathcal{P}(I_{\bar{a}})} \right). \quad (5)$$

where \mathcal{F}^{-1} is inverse Fourier transformation, \mathcal{A} and \mathcal{P} represent the amplitude and phase spectrum, and β controls the strength of style transformation.

Utilizing IST, the generated $\bar{I}_{\bar{a}}$ contains the style patterns of unlabeled image and also has correct spatial correspondence with the pseudo mask $S_{\bar{a}} = S_a \circ \phi$. Therefore, the seg-model can be trained with the image-mask pairs $(\bar{I}_{\bar{a}}, S_{\bar{a}})$.

However, mixing $\mathcal{A}(I_{\bar{a}})$ and $\mathcal{A}(I_u)$ induces visual artifacts especially when $I_{\bar{a}}$ and I_u are incorrectly aligned. As evidenced in Fig. 3, it causes visual artifacts for misaligned images, and this side effect gets worse on those misaligned regions as the transformation strength β goes higher.

To address this, StyleSeg V2 adopts the most intuitive but effective solution that dynamically lowers the style transformation strength β according to the registration errors, i.e., the confidence map C . Therefore, an improved IST is proposed and called weighted image-aligned style transformation (WIST) as depicted in Fig. 4. Specifically, we firstly acquire N binary masks utilizing a series of gate functions through the formula:

$$M_n(x, y, z) = \begin{cases} 1, & \text{if } \frac{n}{N} \leq C(x, y, z) < \frac{n+1}{N} \\ 0, & \text{otherwise.} \end{cases} \quad (6)$$

where $n = 0, \dots, N - 1$ and (x, y, z) is a voxel index.

Then we multiply the I_u and $I_{\bar{a}}$ with M_n to separate them into multiple regions with different registration confidence. We perform IST on the M_n -extracted regions using β_n , which is randomly sampled from the interval $[\frac{n}{N}, \frac{n+1}{N})$ and finally add all results together to obtain the weighted style-transformed atlas image $\bar{I}_{\bar{a}}$.

Utilizing WIST, the generated $\bar{I}_{\bar{a}}$ will have less artifacts even when the reg-model has large registration errors in the

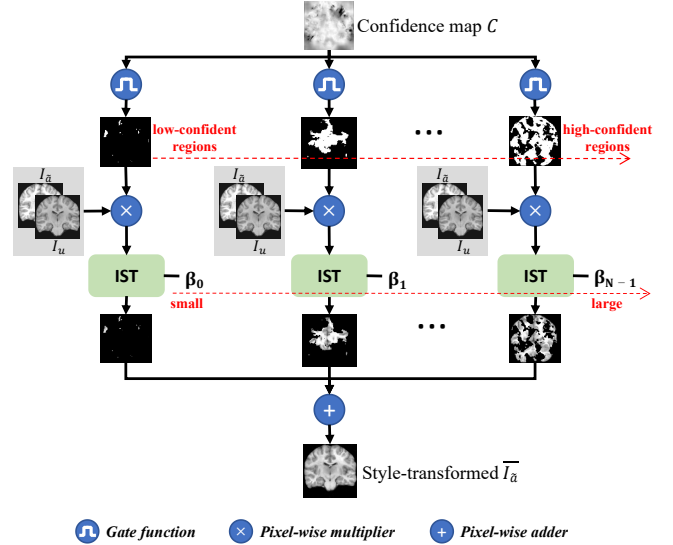


Fig. 4: The detail of weighted IST (WIST), which divides the warped atlas $I_{\bar{a}}$ and unlabeled I_u images into multiple sub-images with different confidence intervals, and applies smaller style-transformation strength on the sub-images with lower confidence, and vice versa. The style-transformed sub-images are added together to give the final WIST-transformed warped atlas image $\bar{I}_{\bar{a}}$.

initial stage of iteration. Thus, we can trustfully feed $\bar{I}_{\bar{a}}$ into seg-model to predict a mask $\hat{S}_{\bar{a}}$ and constrain the seg-model with the loss $\mathcal{L}_d = -Dice(\hat{S}_{\bar{a}}, S_{\bar{a}})$, where $Dice(\cdot, \cdot)$ is the Dice coefficient and can be formulated as:

$$Dice(A, B) = \frac{2|A \cap B|}{|A| + |B|}. \quad (7)$$

3.4 Confidence guided Dice loss of unlabeled images

The original StyleSeg did not directly use the unlabeled images for segmentation training since the pseudo mask $S_{\bar{a}}$ and the unlabeled image I_u spatially mismatch. Under the guidance of the registration confidence C , StyleSeg V2 can suppress the mis-aligned regions in the segmentation results of I_u and $S_{\bar{a}}$, and thus encourages the seg-model to more focus on the regions where the pseudo mask is more reliable. Therefore, the confidence guided Dice-loss is defined as follows for supervising the seg-model using unlabeled images:

$$\mathcal{L}_{cgd} = -Dice(C\hat{S}_u, CS_{\bar{a}}). \quad (8)$$

where \hat{S}_u is the segmentation result of I_u predicted by seg-model. Using the \mathcal{L}_{cgd} , the unlabeled images can also be utilized, which reduces the data waste and further boosts the seg-model.

3.5 Implementation and training details

Registration constraints

In the initial phase, StyleSeg V2 trains the reg-model in an unsupervised manner using two losses \mathcal{L}_{IC} and \mathcal{L}_{smo} . \mathcal{L}_{IC} is Normalization Local Correlation Coefficient (NLCC) between $I_{\bar{a}}$ and I_u , that is, $\mathcal{L}_{IC} = -NLCC(I_{\bar{a}}, I_u)$. \mathcal{L}_{smo}

is a regular term to constrain the smoothness of displacement field, which is formulated as $\mathcal{L}_{Smo} = \|\nabla\phi\|_2^2$.

In the subsequent training of the reg-model, we additionally utilize a loss \mathcal{L}_{weak} as an auxiliary weak-supervision term to improve the registration performance on the regions of interest. \mathcal{L}_{weak} constrains the pseudo mask $S_{\hat{a}}$ of unlabeled image predicted by reg-model to be consistent with the refined one \hat{S}_u predicted by the frozen seg-mode, that is, $\mathcal{L}_{weak} = -Dice(S_{\hat{a}}, \hat{S}_u)$.

Therefore, the whole loss function can be formulated as:

$$\mathcal{L}_{Reg}^i = \begin{cases} \mathcal{L}_{IC} + \mathcal{L}_{Smo}, & \text{if } i = 0 \\ \mathcal{L}_{IC} + \mathcal{L}_{weak} + \mathcal{L}_{Smo}, & \text{if } i \geq 1. \end{cases} \quad (9)$$

where i indexes the iterations and 0 means the initial phase. In our experiment, we utilize 3 iterations of training to get the final model.

Segmentation constraints

We use two losses \mathcal{L}_d and \mathcal{L}_{cgd} as explained in Sec. 3.3 and Sec. 3.4, respectively, for supervising the seg-model. The whole loss function can be calculated as:

$$\mathcal{L}_{Seg} = \mathcal{L}_d + \lambda\mathcal{L}_{cgd}, \quad (10)$$

where λ is set to 0.5 in our experiment.

The learning rate is set to 1×10^{-4} and 1×10^{-3} for reg-model and seg-model respectively. We perform random spatial transformations including affine, B-spline transformations for data augmentation. We implement our method based on TensorFlow [Abadi *et al.*, 2016] and use the Adam optimizer to train the network using a single GPU resource of NVIDIA RTX A6000 with 48-GB memory.

4 Experiments

4.1 Datasets and Evaluation Metrics

We use two brain MRI datasets OASIS [Marcus *et al.*, 2007] and CANDIShare [Kennedy *et al.*, 2012] and one heart CT dataset MH-WHS 2017 [Zhuang and Shen, 2016] for evaluation and comparison in this work.

OASIS contains 414 scans of T1 brain MRI with ground-truth (GT) mask of 35 brain tissues. All brain MRI images are pre-processed to remove the skull, corrected the bias field and rigid-aligned.

CANDIShare contains 103 scans of T1 brain MRI with multiple brain structures. We select 28 brain tissues following [Wang *et al.*, 2020] for a fair comparison. We perform the same data pre-processing of OASIS on this dataset.

MM-WHS 2017 contains 20 labeled heart CT images with the GT mask of 7 big cardiac structures, and 40 unlabeled images. The images are also rigid-aligned with each other using the similar data pre-processing.

For the brain MRI datasets, we randomly divide the data in each dataset into training and test sets, obtaining 331 training and 83 test images in OASIS, and 83 training and 20 test images in CANDIShare. We select an image from the training set as atlas in both OASIS and CANDIShare by following [Wang *et al.*, 2020; Puonti *et al.*, 2016], and the rest of the training set is viewed as unlabeled images. For the CT heart images, the 40 unlabeled images are used as the training set,

and a labeled image is randomly selected as atlas and the rest 19 are viewed as the test set.

We use Dice score and Hausdorff Distance (HD) as evaluation metrics. The calculation of Dice is formulated in Eq. (7). The Hausdorff Distance measures the maximum mismatch between surfaces of two volumes, which is formulated as:

$$HD(A, B) = \max_{a \in A} \left\{ \min_{b \in B} \{ \|a - b\| \} \right\}. \quad (11)$$

where A and B indicate all voxels on the surfaces of two volumes respectively.

4.2 Comparison with the state-of-the-arts

Performance of Seg-model

We first compare the seg-model’s performance of StyleSeg V2 with 5 state-of-the-art dual-model learning methods, i.e., Brainstorm [Zhao *et al.*, 2019a], DeepAtlas [Xu and Niethammer, 2019], PC-Reg-RT [He *et al.*, 2021], BRBS [He *et al.*, 2022] and StyleSeg [Lv *et al.*, 2023]. We directly utilize their released source code for comparison.

Table 1 shows the average Dice score and Hausdorff distance of seg-model on OASIS, CANDIShare and MM-WHS 2017 datasets. As can be seen, StyleSeg V2 outperforms all comparison methods by different margins. Benefit from the new ability of registration error perception, StyleSeg V2 exceeds its previous version StyleSeg by increasing Dice by 2.0%, 2.4%, and 1.7% on the three datasets, respectively. We also visualize the segmentation results of all comparison methods on the three datasets in Fig. 5. From the regions highlighted in the boxes, we can observe that the predicted masks of StyleSeg V2 are most consistent with GT across different modalities and organs.

Performance of Reg-model

The seg-model is good at specific regions, while the reg-model also matters when facing the registration-based tasks like intraoperative navigation and arbitrary tissue segmentation. Therefore, we also evaluate the reg-model of StyleSeg V2, and additionally include 7 state-of-the-arts of registration for comparison. The evaluation is performed by viewing these comparison registration models as atlas-based segmentation, and also using Dice and HD of labeled regions as evaluation metrics. Table 2 lists the comparison results, where some state-of-the-art architectures for merely brain registration, i.e., Elastix [Klein *et al.*, 2009], VoxelMorph [Balakrishnan *et al.*, 2019], 10*VTN [Zhao *et al.*, 2019b] and PCNet [Lv *et al.*, 2022], are also included.

As can be seen, the reg-model of StyleSeg V2 outperforms that of the original StyleSeg by increasing Dice by 0.7%, 1.6% and 1.6% respectively and greatly exceeds other registration and dual-model learning methods. Besides, we observe that the segmentation performances of other dual-model learning methods are almost on par with, and even inferior to the pure registration methods (the first four rows). On contrary, StyleSeg V2 can achieve ‘win-win’ results of both seg-model and reg-model, showing greater potentials for both segmentation of specific brain tissues and other registration-based applications.

Method	OASIS		CANDIShare		MM-WHS 2017	
	Dice \uparrow	HD \downarrow	Dice \uparrow	HD \downarrow	Dice \uparrow	HD \downarrow
Brainstorm	0.813 \pm 0.018	1.651 \pm 0.327	0.827 \pm 0.015	2.133 \pm 0.415	0.825 \pm 0.044	7.455 \pm 2.354
DeepAtlas	0.819 \pm 0.018	1.659 \pm 0.330	0.828 \pm 0.014	2.059 \pm 0.415	0.849 \pm 0.039	6.187 \pm 2.060
PC-Reg-RT	0.764 \pm 0.025	2.846 \pm 0.533	0.829 \pm 0.013	2.260 \pm 0.278	0.868 \pm 0.029	5.364 \pm 1.917
BRBS	0.835 \pm 0.009	1.622 \pm 0.270	0.851 \pm 0.007	1.882 \pm 0.305	0.892 \pm 0.020	5.551 \pm 2.084
StyleSeg	0.851 \pm 0.017	1.509 \pm 0.307	0.839 \pm 0.012	1.982 \pm 0.275	0.886 \pm 0.024	4.923 \pm 1.271
StyleSeg V2	0.868 \pm 0.004	1.513 \pm 0.247	0.859 \pm 0.007	1.711 \pm 0.289	0.901 \pm 0.019	4.531 \pm 1.382

Table 1: Comparison results of seg-model on the three datasets. The best performance is marked in bold

Method	OASIS		CANDIShare		MM-WHS 2017	
	Dice \uparrow	HD \downarrow	Dice \uparrow	HD \downarrow	Dice \uparrow	HD \downarrow
Elastix	0.750 \pm 0.019	1.852 \pm 0.354	0.785 \pm 0.016	2.232 \pm 0.348	0.746 \pm 0.102	9.639 \pm 4.901
VoxelMorph	0.787 \pm 0.019	1.625 \pm 0.271	0.802 \pm 0.018	2.229 \pm 0.430	0.811 \pm 0.046	7.850 \pm 2.584
10*VTN	0.798 \pm 0.018	1.497 \pm 0.278	0.805 \pm 0.015	2.092 \pm 0.319	0.874 \pm 0.023	6.640 \pm 1.872
PCNet	0.808 \pm 0.014	1.453 \pm 0.250	0.812 \pm 0.013	2.110 \pm 0.347	0.850 \pm 0.040	6.794 \pm 2.482
Brainstorm	0.782 \pm 0.024	1.674 \pm 0.331	0.800 \pm 0.026	2.325 \pm 0.599	0.812 \pm 0.044	7.268 \pm 2.142
DeepAtlas	0.800 \pm 0.019	1.638 \pm 0.303	0.818 \pm 0.014	2.096 \pm 0.328	0.843 \pm 0.041	6.654 \pm 2.190
PC-Reg-RT	0.731 \pm 0.033	2.072 \pm 0.376	0.819 \pm 0.013	2.132 \pm 0.355	0.832 \pm 0.042	6.587 \pm 1.980
BRBS	0.796 \pm 0.011	1.579 \pm 0.211	0.824 \pm 0.009	2.044 \pm 0.329	0.879 \pm 0.023	5.099 \pm 1.346
StyleSeg	0.841 \pm 0.016	1.520 \pm 0.272	0.831 \pm 0.013	1.981 \pm 0.279	0.880 \pm 0.025	5.102 \pm 1.455
StyleSeg V2	0.847 \pm 0.004	1.330 \pm 0.239	0.844 \pm 0.005	1.928 \pm 0.297	0.894 \pm 0.020	4.647 \pm 1.453

Table 2: Comparison results of reg-model on the three datasets. The other four state-of-the-art registration methods are included in the first four rows. The best performance is marked in bold

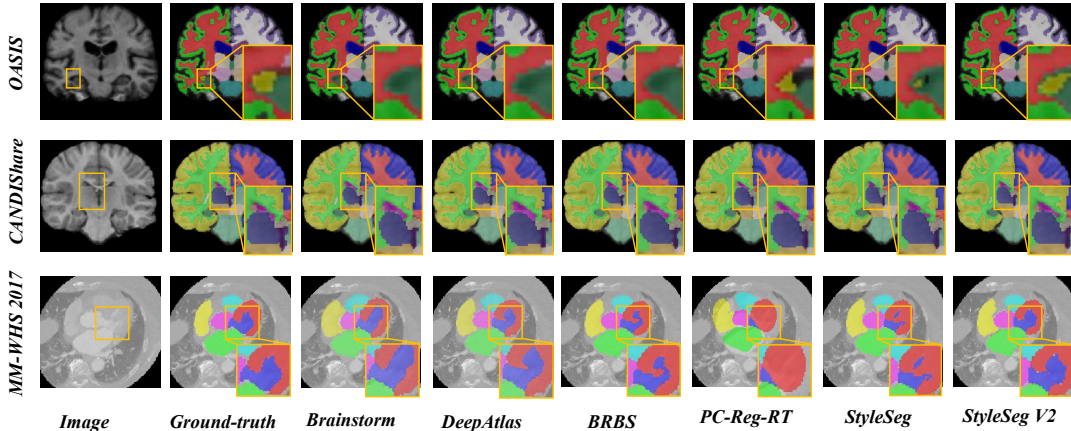


Fig. 5: The visualization results of different dual-model based one-shot segmentation methods (the seg-model part) on the three datasets.

4.3 Ablation studies

We conduct ablation studies on OASIS to verify the effectiveness of our proposed two modules enabled by the perceived registration errors, i.e., WIST and \mathcal{L}_{cgd} , and also to explore the impact of division quantity N on WIST.

Effectiveness of WIST and \mathcal{L}_{cgd}

To verify the effectiveness of WIST and \mathcal{L}_{cgd} , We train three variants of StyleSeg V2, denoted as “StyleSeg”, “StyleSeg+WIST”, and “StyleSeg+ \mathcal{L}_{cgd} ”, by disabling WIST and/or \mathcal{L}_{cgd} . The StyleSeg V2 itself is actually “StyleSeg+WIST& \mathcal{L}_{cgd} ”. If disabling WIST, we use the original IST for style transformation. If disabling \mathcal{L}_{cgd} , we discard the unlabeled images in the segmentation training. We show the performance of reg-model and seg-model at each iteration, and plot the line graphs in Fig. 6.

From Fig. 6, we have four observations:

(i) Comparing the results of “StyleSeg+WIST” with “StyleSeg” in Fig. 6(b), we can observe that after 3 iterations, the seg-model with WIST achieves an improvement of average Dice by 1.6% over the original StyleSeg. This is because WIST can provide more diverse and higher-fidelity style-transformed atlas images than the original IST. Fig. 6 shows exemplar results of IST and WIST, and we can see that the subtle structures generated via IST is damaged by artifacts which may harm the subsequent segmentation learning. In comparison, WIST induces fewer artifacts without sacrificing the effect of style transformation.

(ii) Comparing the results of “StyleSeg+ \mathcal{L}_{cgd} ” with “StyleSeg” in Fig. 6(b), we can observe the seg-model with \mathcal{L}_{cgd} finally achieves an improvement of average Dice by 1.2%. This verifies the non-ignorable value of unlabeled images in the segmentation training, which, however, has to be abandoned

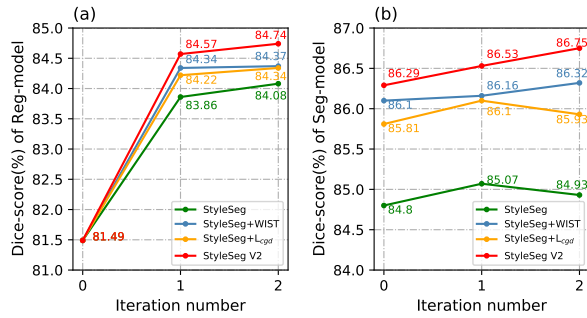


Fig. 6: Line graphs of the average Dice of different variants at each iteration. (a) the line graphs of reg-model, and (b) the line graphs of seg-model.

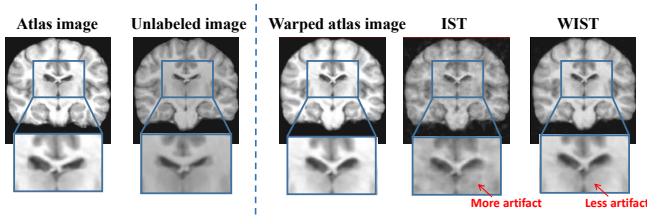


Fig. 7: Comparison result of IST and WIST. By use of WIST, fewer artifacts are produced as highlighted in the blue box.

in the original StyleSeg due to the misalignment caused by the reg-model.

(iii) Comparing the results of “StyleSeg+WIST” with “StyleSeg+L_{cgd}” in Fig. 6(b), we can observe that applying WIST only boosts the segmentation performance more significantly than applying L_{cgd} only. This indicates that the alignment between training image and mask is more important for the dual-model iterative learning. Therefore, addressing the diversity and fidelity of the warped atlas image may be the promising direction to enhance the performance of dual-model based one-shot brain segmentation.

(iv) Comparing the Fig. 6(a) with (b), we can observe that our proposed WIST and L_{cgd} also help to improve the performance of reg-model, which in turn boosts the seg-model during iteration.

The impact of division quantity N on WIST

In WIST, we divide the confidence map C into N parts, but the determination of N is a trade-off: when N is small, the style contrast of different regions becomes intense, yielding visually unreal boundaries, and when N is large, the interval $[\frac{n}{N}, \frac{n+1}{N})$ becomes narrow, and the random selection of the corresponding β_n becomes more certain, which lowers the diversity of style-transformed atlas image.

In view of this, we train 6 variants of StyleSeg V2 with N in WIST set to that uniformly-space sampled from 2 to 22. Fig. 8(a) shows the segmentation performance of seg-model at the first iteration. As can be seen, the seg-model will degrade when employing both too small and too large N value. To explain this phenomenon, we set β_n to the rightmost and leftmost values of each interval to generate two style-transformed atlas images, and calculate their subtraction

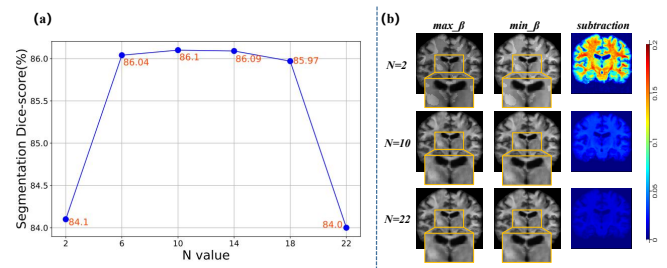


Fig. 8: The impact of different sets of N in WIST. (a) the line graph of seg-model’s Dice at different N , and (b) subtraction images reflecting the diversity of generated style-transformed atlas image (more brighter, more diverse).

tion to reflect the style diversity under different selections of N . Fig. 8(b) shows the style-transformed atlas images using the rightmost and leftmost values as β_n , and their subtraction images. As can be seen, using smaller N provides a greater space where the style varies (brighter subtraction image), but also creates more salient unreal boundaries, which harms the image structures. On the contrary, using larger N produces more realistic image but narrows the style varying space (darker subtraction image). To trade-off the diversity and fidelity, we set N to 10 in StyleSeg V2 by default.

5 Conclusion

In this paper, we propose StyleSeg V2 attempting to eliminate the negative impact caused by registration error, which is ignored by original StyleSeg. We first introduce a optimization-free error perception method, using mirror error to approximate the registration error. We then propose the weighted image-aligned style transformation to produce the aligned image-mask sample with less artifacts, and additionally employ a confidence guided Dice-loss to integrate coarsely-aligned image-mask pairs into segmentation learning. Experiments on two public brain datasets, OASIS and CANDIShare, and one heart dataset, MM-WHS 2017 demonstrate the superior performance of our developed StyleSeg V2 over other state-of-the-art methods. The ablation studies also prove the effectiveness of our proposed two components, i.e., weighted image-aligned style transformation and confidence guided Dice-loss.

References

[Abadi *et al.*, 2016] Martın Abadi, Paul Barham, Jianmin Chen, Zhifeng Chen, Andy Davis, Jeffrey Dean, Matthieu Devin, Sanjay Ghemawat, Geoffrey Irving, Michael Isard, et al. {TensorFlow}: a system for {Large-Scale} machine learning. In *12th USENIX symposium on operating systems design and implementation (OSDI 16)*, pages 265–283, 2016.

[Balakrishnan *et al.*, 2019] Guha Balakrishnan, Amy Zhao, Mert R Sabuncu, John Guttag, and Adrian V Dalca. Voxel-morph: a learning framework for deformable medical image registration. *IEEE transactions on medical imaging*, 38(8):1788–1800, 2019.

- [Beljaards *et al.*, 2020] Laurens Beljaards, Mohamed S Elmahdy, Fons Verbeek, and Marius Staring. A cross-stitch architecture for joint registration and segmentation in adaptive radiotherapy. In *Medical Imaging with Deep Learning*, pages 62–74. PMLR, 2020.
- [Bierbrier *et al.*, 2022] Joshua Bierbrier, Houssein-Eddine Gueziri, and D Louis Collins. Estimating medical image registration error and confidence: A taxonomy and scoping review. *Medical Image Analysis*, page 102531, 2022.
- [Geuze *et al.*, 2005] EEJD Geuze, Eric Vermetten, and James Douglas Bremner. Mr-based in vivo hippocampal volumetrics: 2. findings in neuropsychiatric disorders. *Molecular psychiatry*, 10(2):160–184, 2005.
- [He *et al.*, 2020] Yuting He, Tiantian Li, Guanyu Yang, Youyong Kong, Yang Chen, Huazhong Shu, Jean-Louis Coatrieux, Jean-Louis Dillenseger, and Shuo Li. Deep complementary joint model for complex scene registration and few-shot segmentation on medical images. In *Computer Vision—ECCV 2020: 16th European Conference, Glasgow, UK, August 23–28, 2020, Proceedings, Part XVIII 16*, pages 770–786. Springer, 2020.
- [He *et al.*, 2021] Yuting He, Tiantian Li, Rongjun Ge, Jian Yang, Youyong Kong, Jian Zhu, Huazhong Shu, Guanyu Yang, and Shuo Li. Few-shot learning for deformable medical image registration with perception-correspondence decoupling and reverse teaching. *IEEE Journal of Biomedical and Health Informatics*, 26(3):1177–1187, 2021.
- [He *et al.*, 2022] Yuting He, Rongjun Ge, Xiaoming Qi, Yang Chen, Jiasong Wu, Jean-Louis Coatrieux, Guanyu Yang, and Shuo Li. Learning better registration to learn better few-shot medical image segmentation: Authenticity, diversity, and robustness. *IEEE Transactions on Neural Networks and Learning Systems*, 2022.
- [Kennedy *et al.*, 2012] David N Kennedy, Christian Haselgrove, Steven M Hodge, Pallavi S Rane, Nikos Makris, and Jean A Frazier. Candishare: a resource for pediatric neuroimaging data. *Neuroinformatics*, 10:319–322, 2012.
- [Klein *et al.*, 2009] Stefan Klein, Marius Staring, Keelin Murphy, Max A Viergever, and Josien PW Pluim. Elastix: a toolbox for intensity-based medical image registration. *IEEE transactions on medical imaging*, 29(1):196–205, 2009.
- [Lorenzo-Valdés *et al.*, 2002] Maria Lorenzo-Valdés, Gerardo I Sanchez-Ortiz, Raad Mohiaddin, and Daniel Rueckert. Atlas-based segmentation and tracking of 3d cardiac mr images using non-rigid registration. In *Medical Image Computing and Computer-Assisted Intervention—MICCAI 2002: 5th International Conference Tokyo, Japan, September 25–28, 2002 Proceedings, Part I 5*, pages 642–650. Springer, 2002.
- [Lötjönen *et al.*, 2010] Jyrki MP Lötjönen, Robin Wolz, Juha R Koikkalainen, Lennart Thurfjell, Gunhild Walde- mar, Hilikka Soininen, Daniel Rueckert, Alzheimer’s Disease Neuroimaging Initiative, et al. Fast and robust multi-atlas segmentation of brain magnetic resonance images. *Neuroimage*, 49(3):2352–2365, 2010.
- [Lv *et al.*, 2022] Jinxin Lv, Zhiwei Wang, Hongkuan Shi, Haobo Zhang, Sheng Wang, Yilang Wang, and Qiang Li. Joint progressive and coarse-to-fine registration of brain mri via deformation field integration and non-rigid feature fusion. *IEEE Transactions on Medical Imaging*, 41(10):2788–2802, 2022.
- [Lv *et al.*, 2023] Jinxin Lv, Xiaoyu Zeng, Sheng Wang, Ran Duan, Zhiwei Wang, and Qiang Li. Robust one-shot segmentation of brain tissues via image-aligned style transformation. In *Proceedings of the AAAI Conference on Artificial Intelligence*, volume 37, pages 1861–1869, 2023.
- [Marcus *et al.*, 2007] Daniel S Marcus, Tracy H Wang, Jamie Parker, John G Csernansky, John C Morris, and Randy L Buckner. Open access series of imaging studies (oasis): cross-sectional mri data in young, middle aged, nondemented, and demented older adults. *Journal of cognitive neuroscience*, 19(9):1498–1507, 2007.
- [Mok and Chung, 2022] Tony CW Mok and Albert CS Chung. Unsupervised deformable image registration with absent correspondences in pre-operative and post-recurrence brain tumor mri scans. In *International Conference on Medical Image Computing and Computer-Assisted Intervention*, pages 25–35. Springer, 2022.
- [Puonti *et al.*, 2016] Oula Puonti, Juan Eugenio Iglesias, and Koen Van Leemput. Fast and sequence-adaptive whole-brain segmentation using parametric bayesian modeling. *NeuroImage*, 143:235–249, 2016.
- [Saygili *et al.*, 2015] Gorkem Saygili, Marius Staring, and Emile A Hendriks. Confidence estimation for medical image registration based on stereo confidences. *IEEE transactions on medical imaging*, 35(2):539–549, 2015.
- [Sokooti *et al.*, 2019] Hessam Sokooti, Gorkem Saygili, Ben Glocker, Boudewijn PF Lelieveldt, and Marius Staring. Quantitative error prediction of medical image registration using regression forests. *Medical image analysis*, 56:110–121, 2019.
- [Sokooti *et al.*, 2021] Hessam Sokooti, Sahar Yousefi, Mohamed S Elmahdy, Boudewijn PF Lelieveldt, and Marius Staring. Hierarchical prediction of registration misalignment using a convolutional lstm: Application to chest ct scans. *IEEE Access*, 9:62008–62020, 2021.
- [Wang *et al.*, 2020] Shuxin Wang, Shilei Cao, Dong Wei, Renzhen Wang, Kai Ma, Liansheng Wang, Deyu Meng, and Yefeng Zheng. Lt-net: Label transfer by learning reversible voxel-wise correspondence for one-shot medical image segmentation. In *Proceedings of the IEEE/CVF Conference on Computer Vision and Pattern Recognition*, pages 9162–9171, 2020.
- [Xu and Niethammer, 2019] Zhenlin Xu and Marc Niethammer. Deepatlas: Joint semi-supervised learning of image registration and segmentation. In *Medical Image Computing and Computer Assisted Intervention—MICCAI 2019*:

22nd International Conference, Shenzhen, China, October 13–17, 2019, *Proceedings, Part II* 22, pages 420–429. Springer, 2019.

- [Zhao *et al.*, 2019a] Amy Zhao, Guha Balakrishnan, Fredo Durand, John V Guttag, and Adrian V Dalca. Data augmentation using learned transformations for one-shot medical image segmentation. In *Proceedings of the IEEE/CVF conference on computer vision and pattern recognition*, pages 8543–8553, 2019.
- [Zhao *et al.*, 2019b] Shengyu Zhao, Yue Dong, Eric I-Chao Chang, and Yan Xu. Recursive cascaded networks for unsupervised medical image registration. In *Proceedings of the IEEE/CVF International Conference on Computer Vision (ICCV)*, October 2019.
- [Zhao *et al.*, 2019c] Shengyu Zhao, Tingfung Lau, Ji Luo, I Eric, Chao Chang, and Yan Xu. Unsupervised 3d end-to-end medical image registration with volume tweening network. *IEEE journal of biomedical and health informatics*, 24(5):1394–1404, 2019.
- [Zhuang and Shen, 2016] Xiahai Zhuang and Juan Shen. Multi-scale patch and multi-modality atlases for whole heart segmentation of mri. *Medical image analysis*, 31:77–87, 2016.